Science Advances
AAAS

advances.sciencemag.org/cgi/content/full/4/7/eaar7720/DC1

Supplementary Materials for

Room temperature in-plane ferroelectricity in van der Waals In_2Se_3

Changxi Zheng*, Lei Yu, Lin Zhu, James L. Collins, Dohyung Kim, Yaoding Lou, Chao Xu, Meng Li, Zheng Wei, Yupeng Zhang, Mark T. Edmonds, Shiqiang Li, Jan Seidel, Ye Zhu, Jefferson Zhe Liu, Wen-Xin Tang*, Michael S. Fuhrer*

*Corresponding author. Email: changxi.zheng@monash.edu (C.Z.); wenxintang@cqu.edu.cn (W.-X.T.); michael.fuhrer@monash.edu (M.S.F.)

Published 13 July 2018, *Sci. Adv.* **4**, eaar7720 (2018)
DOI: 10.1126/sciadv.aar7720

This PDF file includes:

X-ray diffraction (XRD) spectrum

Figure S1 shows the room temperature XRD spectrum of In_2Se_3 crystals exfoliated on a PDMS substrate. Based on the peak positions, the crystal structure of our In_2Se_3 crystal is β phase with $R\bar{3}m$ space group (JCPDS 35–1056) and lattice constants of a = 4.000 Å, c = 28.33 Å (*23*). As shown by the peak indices in Fig. S1, the XRD spectrum of our sample only identifies the c-axis lattice constant due to direction of the scan. Thus, an atomic distortion parallel to the c-plane would not be detected.

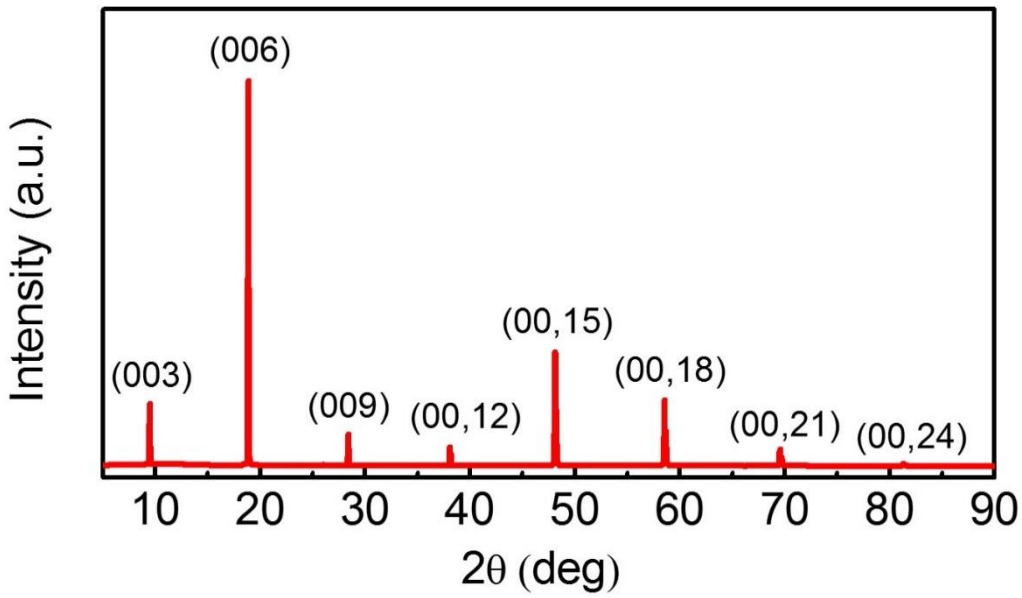

Fig. S1. X-ray diffraction spectrum of In_2Se_3 flakes at room temperature.

Air stability of In_2Se_3 and domains

Figure S2A shows the optical image of a large area In_2Se_3 flake freshly exfoliated, and Fig. S2B shows the atomic force microscopy (AFM) image and height profile of the same flake. As with previous report (*28*), we were not able to obtain monolayer In_2Se_3 by mechanical exfoliation. This probably implies the van der Waals interaction is stronger in In_2Se_3 than that in graphene. Figure S2C shows an optical micrograph

using linearly polarized light, showing the domains. The domains of the flake are stable in air at room temperature; no observable change happens after 7 days (Fig. S2D) and 60days (Fig. S2E).

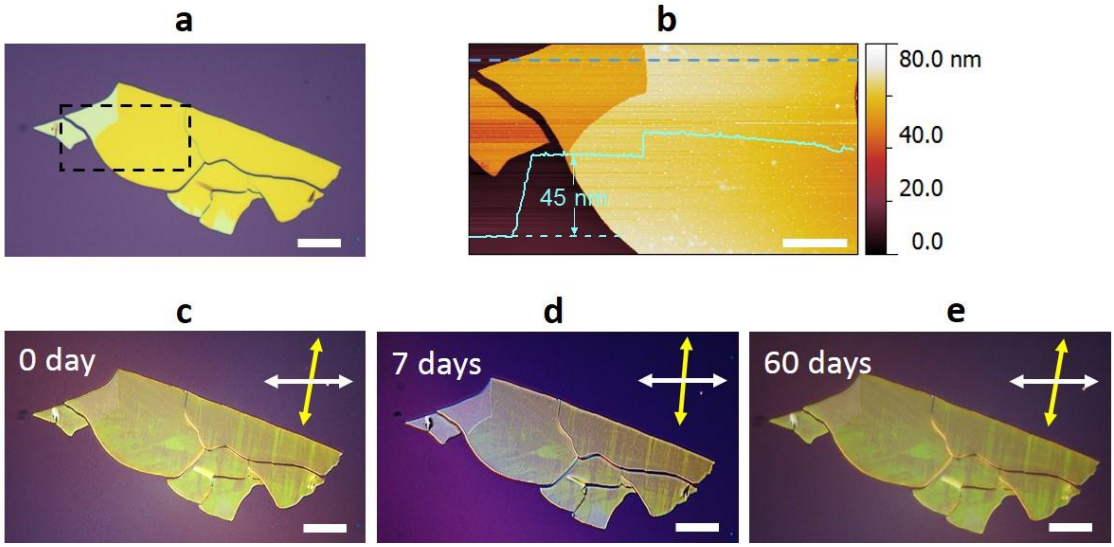

Fig. S2. Air stability of In_2Se_3 and domains. (**A**), Optical image of a freshly exfoliated thin flake of In_2Se_3 using unpolarized illumination. (**B**) Atomic force microscope topograph of the region inside the dashed rectangle shown in (**A**). The height profile is taken along the dashed line. Scale bar: 5 μm. (**C-E**), Optical images of the flake after different periods of air exposure, with linearly polarized illumination and detection. The up-down arrow (yellow) represents the linear polarization direction of incident light and the left-right arrow (white) represents the linear polarization direction of the analyser to reflected light. The scale bars in (**A**, **C-E**) are 10 μm.

Low energy electron microscopy (LEEM) characterizations

LEEM is a powerful characterization technique to inspect the surface morphology of material (*40*). Figure S3 presents the LEEM images of a freshly exfoliated In_2Se_3 surface taken by either the perpendicular (left) or the tilted (right) electron beam at 9.9

eV. Generally, the surface is flat and clean except some pinholes on top. However, no domain structure is observed when the electron beam is incident perpendicularly on the surface. While the surface is illuminated by the tilted electron beam, the domain contrast appears (*40*).

In order to understand the mechanism of image contrast which is determined by the characteristics of domains, we first calibrate the tilt of the beam in our apparatus. In LEEM, the tilt angle and direction of the electron beam can be controlled by the currents of the beam tilt coils which are denoted as Tilt X and Tilt Y. Figure S4A presents a set of low energy electron diffraction patterns obtained on In_2Se_3 surface with different values of Tilt X and Tilt Y. In the images, the bright spot is the (00) beam and the circle is the contrast aperture applied for bright field imaging. The (00) beam shifts linearly along the X (Y) direction as a function of Tilt X (Tilt Y) current, see Fig. 4B. Thus, by using a set of Tilt X and Tilt Y values, the electron beam can be controlled to rotate uniformly at different azimuth angles and produce a series of images.

We now discuss the imaging of the sample with tilted electron beam. The measurement configuration is shown schematically in Fig. S5A. Figure S5B presents three typical LEEM images taken by the tilted electron beam at the azimuth angle of 90˚, 180˚, and 270˚, respectively. Here, the azimuth angle of 0˚ is defined as the direction along x axis which is perpendicular to the length of the domain, see Fig. S5A and the inset in panel B. Figure S5C plots the intensity profiles taken along the blue lines shown in Panel B. The contrast difference between the two types of domains reverses when the azimuth angle changes from 90˚ to 270˚. Meanwhile, the contrast

disappears when the azimuth angle is at 180˚ or 0˚. Figure S5D shows the intensity difference as a function of azimuth angle.

As shown in Fig. 1 of the main text, the domains show linear-dichroic characteristics. Additionally, Fig. 2 indicates the domains are superstructures with different orientations along the high symmetric directions. Based on the information, we here assume the domains are ferroelectric domains due to the shift of atoms in a unit cell. It is known that the maximum light absorption happens when the light polarization direction is parallel to the spontaneous polar direction of the ferroelectric domain. Thus, there are two possibilities of the domain polarization, see Fig. S6. Since the contrast between the two types of domains appears when the electron beam is tilted at certain angles, the contrast is due to the diffraction contrast. Here we use the Howie-Whelan Equations developed for transmission electron microscopy (TEM) to interpret the image contrast between the two types of domains (*41*). The Howie-Whelan Equations are given below

$$\frac{d\phi_0}{dz} = \frac{\pi i}{\xi_g}\phi_g \exp(2\pi i \boldsymbol{g}\cdot\boldsymbol{R}),$$

and

$$\frac{d\phi_g}{dz} = \frac{\pi i}{\xi_g}\phi_o \exp(-2\pi i \boldsymbol{g}\cdot\boldsymbol{R}) + 2\pi i s\phi_g,$$

where ϕ_0 and ϕ_g are the amplitudes of incident beam and (00) beam, z is the electron beam penetration depth, $\boldsymbol{g}$ is the diffraction vector defined as the vector between the incident beam and the diffracted beam in the reciprocal space, $\boldsymbol{R}$ is the displacement of atoms from their reference positions in a unit cell, ξ_g is the extinction distance for the diffracted beam g, and s is the excitation error or deviation parameter. Here, we assume a perfect alignment with $s = 0$. Thus, we see contrast between the domains because the atomic displacement, $\boldsymbol{R}$, is different in different domains, which causes different phase shifts $\alpha = 2\pi \boldsymbol{g} \cdot \boldsymbol{R}$. For example, if we choose one domain with the atomic displacement $\boldsymbol{R_1}$ as a reference, then other domains with the atomic displacement $\boldsymbol{R_2}$ will give an extra phase shift $\alpha = 2\pi \boldsymbol{g} \cdot (\boldsymbol{R_2} - \boldsymbol{R_1})$ for the electron beam and thus will show different image intensities, i.e., image contrast. The contrast disappears when $\alpha = 0$, of which the azimuth angle is either 0^o or 180^o in our coordinate system, see Fig. S5D. The intensity difference can be qualitatively given by $\frac{I_A - I_B}{I_A + I_B} \propto \alpha \propto \cos(\varphi - 90^o) = \sin\varphi$, where I_A and I_B are the intensities of domains A and B at the azimuth angle φ, respectively. The blue dotted curve shown in Fig. S5D is the fitting curve using a sine function. Based on the information, Possibility I presented in Fig. S6 is the case of spontaneous polarization in the ferroelectric domains.

Previously, the low energy electron beam based imaging techniques applied to the study of ferroelectric materials include LEEM and mirror electron microscopy (MEM) (*42-44*). The contrast of domains polarized *out-of-plane* is strong when the surface is imaged by very low energy electrons due to the large work function difference between domains with different polar directions (*43*). On the other hand, for in-plane ferroelectric such as $BaTiO_3$(001), no contrast was observed between domains

(consistent with our observations with untilted beam) except for weak contrast at domain walls (*45*). The formation of weak contrast at domain walls can be understood because the trajectories of imaging electrons hitting at the domain walls are deflected by the electric dipoles perpendicular to the walls. In addition to the contrast, the domain polarization can be switched by low energy electrons. However, in our experiments, we did not observe the domain wall contrast and the domain switch behaviour caused by low energy electrons. There are at least two reasons. Firstly, a ferroelectric domain of In_2Se_3 is formed by one-dimensional superstructures aligning along the same direction. The domain wall of In_2Se_3 may not as sharp as that of $BiTiO_3$(001). As a result, we cannot see contrast of domain wall of In_2Se_3 using perpendicular electron beam. Secondly, In_2Se_3 is a semiconductor with band gap of ~1eV which is much smaller than that of $BiTiO_3$ (*46, 47*). Thus, the electric field accumulated on In_2Se_3 by the illumination electrons is not as strong as that of $BiTiO_3$(001) due to the increased conductivity of In_2Se_3. Therefore, our developed imaging technique using the rotatory tilted electron beam is a powerful technique able to provide clear domain contrast at appropriate tilting angle of electron beam and even to determine the polarization of each domain.

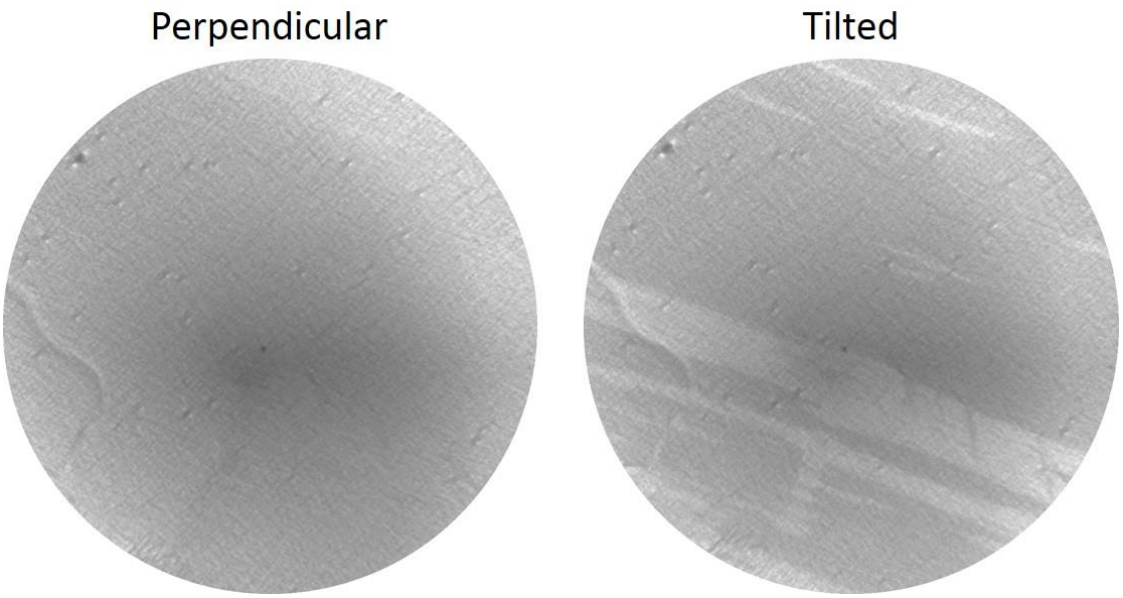

Fig. S3. Image contrast of domains under a tilted electron beam in LEEM. LEEM images of the same In_2Se_3 surface taken using perpendicular (left) or tilted (right) electron beam at 9.9 eV. The field of view (FoV) is10 μm.

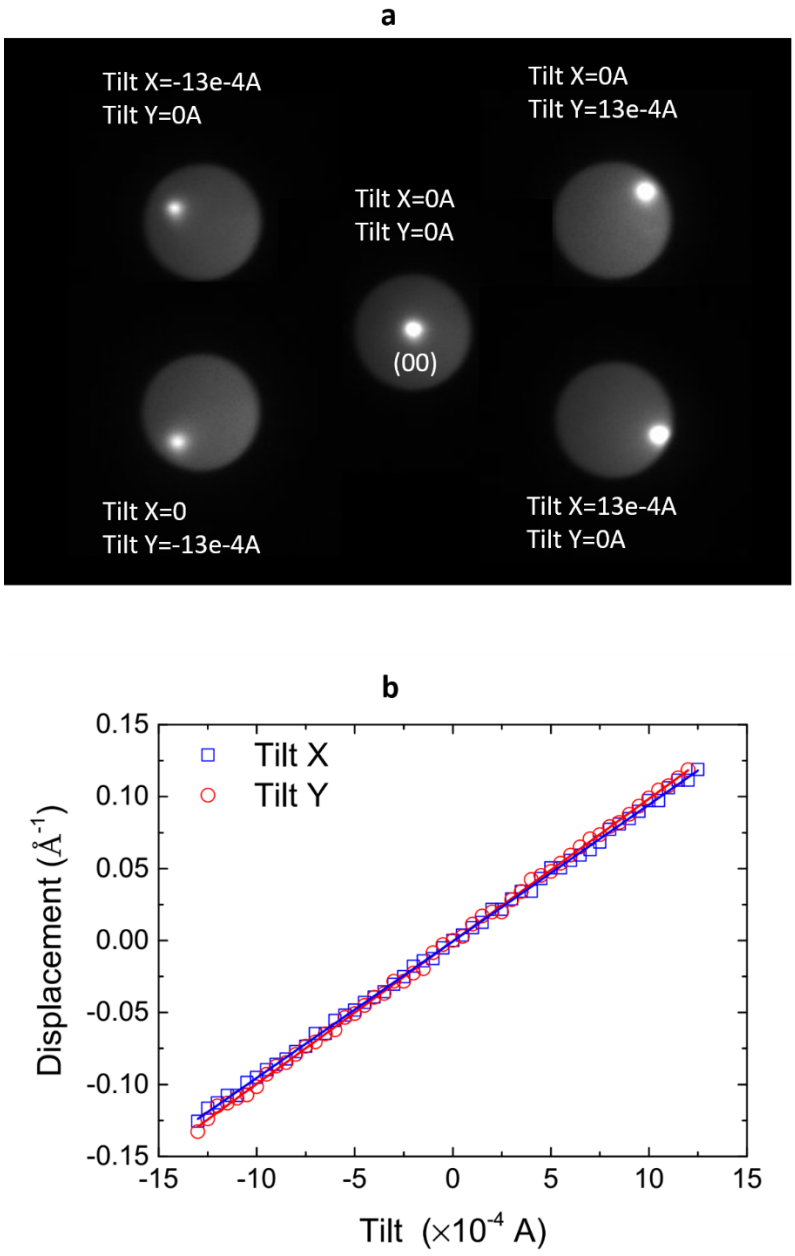

Fig. S4. The control of electron beam tilt in LEEM. (**A**) Low energy electron diffraction (LEED) pattern of In_2Se_3 taken at 9.9 eV. The circle is contrast aperture. The shift of (00) beam is due to the change of beam tilt current. (**B**) Displacement of (00) beam in reciprocal space as a function of beam tilt current.

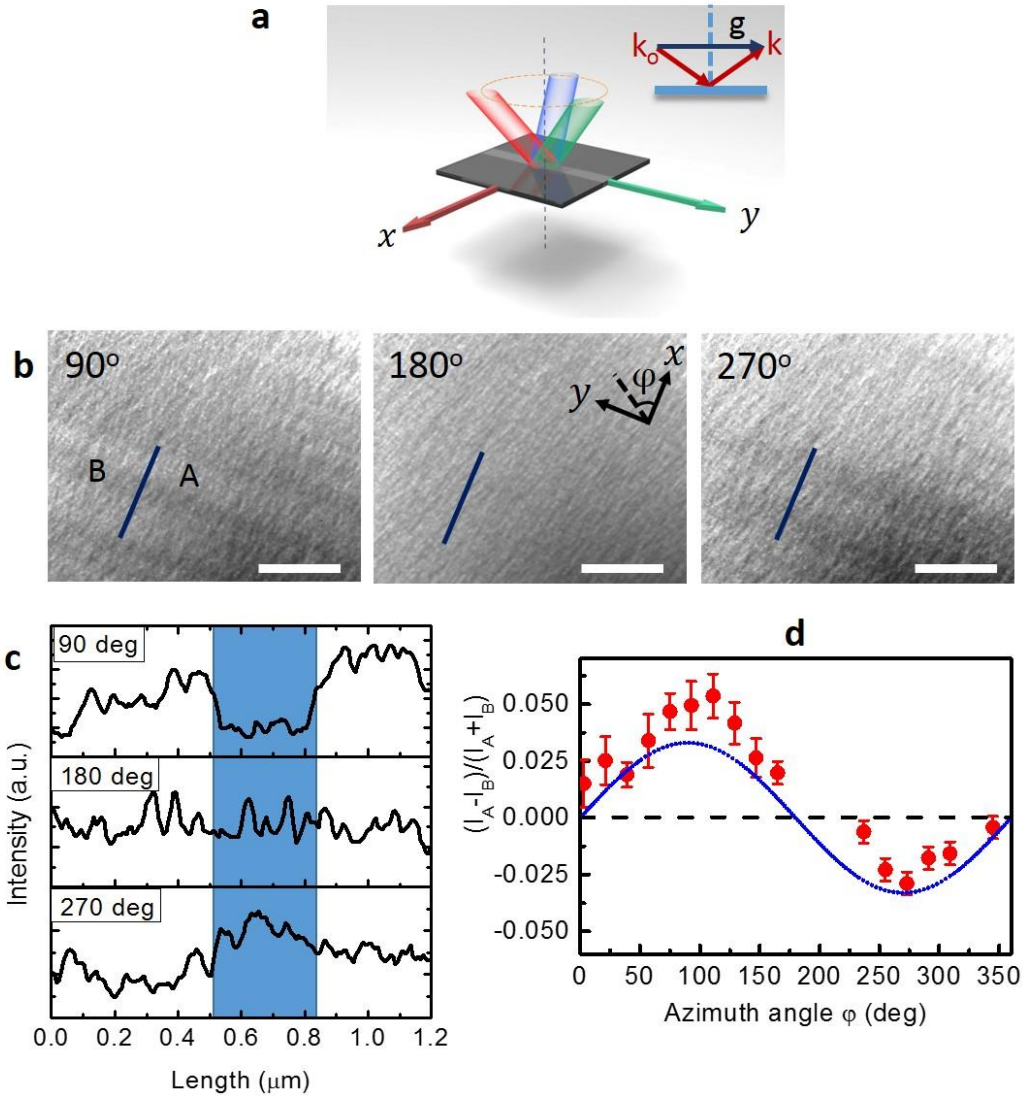

Fig. S5. Tilt angle–dependent domain contrast. (**A**) Schematic of the domains on In_2Se_3 surface imaged by a rotated electron beam at a fixed tilting angle. Inset: the relationship between the incident wave vector $\mathbf{k_o}$ and the reflected wave vector **k** of the electron beams and their vector difference $\boldsymbol{g}$. (**B**) Representative LEEM images of the surface taken by a tilted electron beam at the azimuth angles of 90°, 180° and 270°, respectively. The reverse and the disappearance of the domain contrast are observed. The inset defines the azimuth angle φ. (**C**) The corresponding intensity profiles of the domains taken along the straight lines shown in (**B**). (**D**) The intensity difference

between the domains as a function of the azimuth angle. The blue dotted line is a fitting curve of a sine function. Scale bars are 1 μm across.

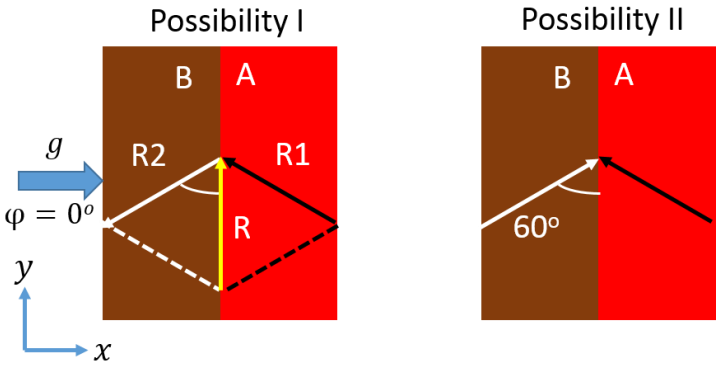

Fig. S6. Proposed ferroelectric polarizations between the two types of domains.

Transmission electron microscopy (TEM) measurements

In_2Se_3 crystals were thinned by acetone sonication for 1 hour. The thin crystals contained in acetone solution were drop casted on a TEM grid. The TEM measurements were carried out using 200 kV at room temperature.

The TEM image shows well aligned one-dimensional periodic stripes in In_2Se_3 at room temperature, see Fig. S7A. The existence of the 1D stripes gives rise to superstructure reflections in the diffraction pattern (Fig. S7C) which is similar to the LEED patterns in Fig. 2B. A high resolution TEM (HRTEM) image (Fig. S7B), corresponding to the yellow square region in Fig. S7A, indicates that one period of the superstructure consisting of the 1.6 nm and 2 nm wide regions along the Se-Se direction. The observation is in coincidence with our cryo-scanning tunneling microscopy analysis shown in Fig. 5C.

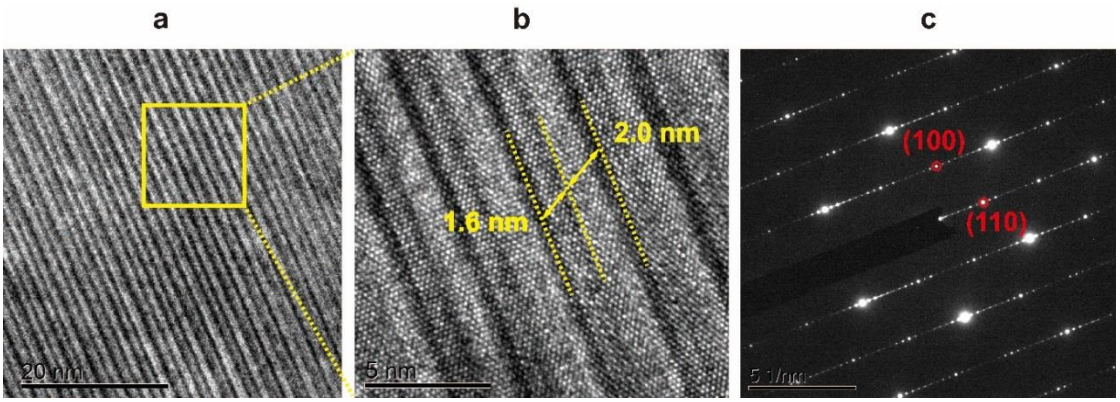

Fig. S7. TEM measurements. (**A**) Bright-field TEM image of β'-In_2Se_3 nano flakes. (**B**) High-resolution TEM image of the region in the yellow square in (**A**). (**C**) Selective area electron diffraction (SAED) patterns of the striped structure.

Polarization calculations using Berry phase method

It is well known that Berry phase expression is a multivalued function. We should be careful to ensure our calculated ferroelectric value is not affected by this issue. We adopt a linear interpolation method between the centrosymmetric phase structure (reference phase with notation 0) and the relaxed polar configuration (ferroelectric phase with notation 6). Five transition state structures were built to calculate the polarization value of In_2Se_3 along the pathway. A smooth curve of polarization without any breaking or jumping points is shown in Fig. S8. This clearly shows that the multivalued function issue of Berry phase method does not affect our results.

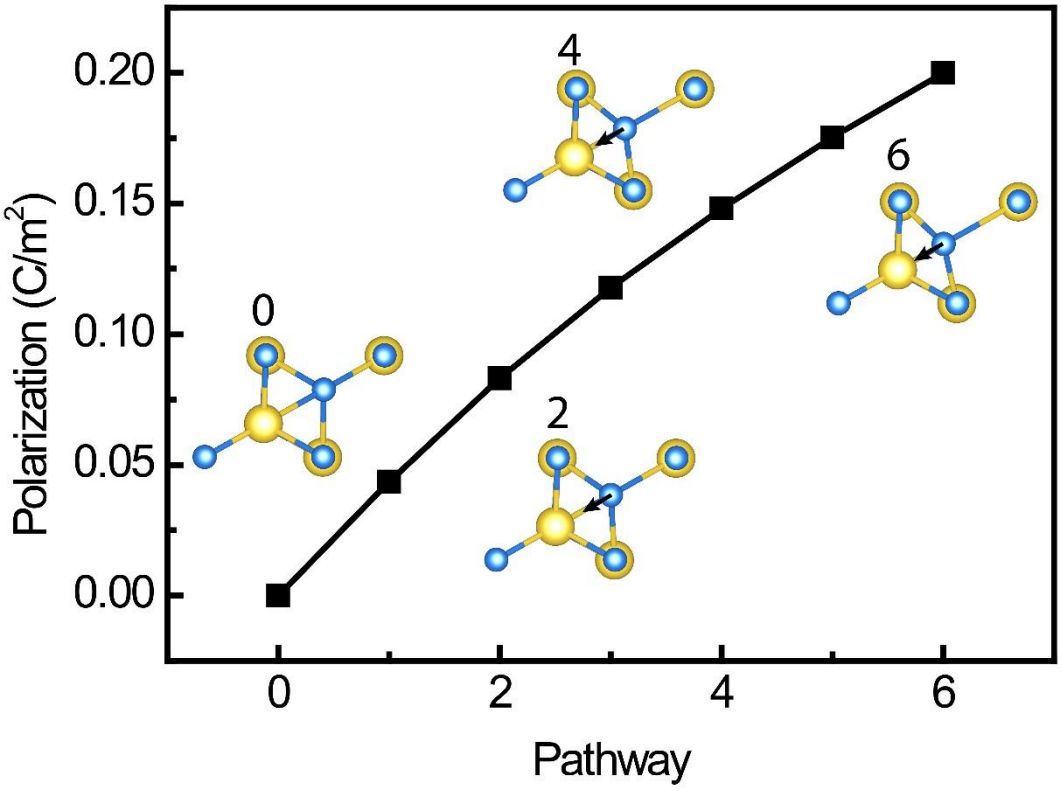

Fig. S8. Ferroelectric polarization calculated using Berry phase method along a pathway connecting the centrosymmetric reference structure (notation 0) and the fully relaxed ferroelectric configuration (notation 6). A linear interpolation method is adopted to generate five intermediate structures along the path. The black arrows indicate the shift direction of the Se atom.